Supporting Information

Mitigating Cathodic Dissolution through Interfacial Water Masking to Enhance the Longevity of Aqueous Zinc-Ion Batteries

Wei Zhong, [a, b, c †] Zeyu Shen, [a, b, †] Jiale Mao, [a, b] Shichao Zhang, [a] Hao Cheng, [a, b, c, *] Yoonseob Kim, [d, e] and Yingying Lu [a, b, c, *]

[a] *State Key Laboratory of Chemical Engineering, Institute of Pharmaceutical Engineering, College of Chemical and Biological Engineering, Zhejiang University, Hangzhou 310027, China.*

[b] *ZJU-Hangzhou Global Scientific and Technological Innovation Center, Zhejiang University, Hangzhou 311215, China.*

[c] *Institute of Wenzhou, Zhejiang University, Wenzhou 325006, China.*

[d] *Department of Chemical and Biological Engineering, The Hong Kong University of Science and Technology, Hong Kong SAR, China.*

[e] *Energy Institute, The Hong Kong University of Science and Technology, Hong Kong SAR, China.*

[*] E-mail: Bob_hao@zju.edu.cn (Hao Cheng); yingyinglu@zju.edu.cn (Yingying Lu)

1. Experimental Section

Materials

The salt $Zn(OTf)_2$ (98%) was procured from Shanghai Macklin Biochemical Co., Ltd. V_2O_5 (98%) and isosorbide dimethyl ether (IDE) (98%) were acquired from Aladdin reagent Co., Ltd.

Electrolyte Preparation

The IDEx (x:20, 30, 40, or 50) electrolytes were prepared by dissolving 2M $Zn(OTf)_2$ into a mixture consisting of (1-x) vol% H_2O and x vol% IDE. For instance, electrolytes with 0 vol% and 20 vol% IDE were designated as IDE0 and IDE20, respectively.

Preparation of Cathode

The $V_2O_5 \cdot nH_2O$ (VOH) cathode materials were synthesized by reacting 1.456 g V_2O_5 powder with 6.4 mL of 30% H_2O_2 in 80 mL of deionized water. The V_2O_5 powder readily dissolved, forming a deep red solution. After resting for 10 hours, the $V_2O_5 \cdot nH_2O$ deposits were collected, thoroughly washed with water, and freeze-dried for 12 hours. The $Zn_{0.25}V_2O_5 \cdot nH_2O$ (ZVO) cathode materials were synthesized through a hydrothermal approach. Generally, a mixed solvent (70 mL of deionized water, 5 mL of acetone, and 2 mL of 10% HNO_3) was used to dissolve 0.54 g of V_2O_5 and 0.43 g of $Zn(OAc)_2$. The autoclave was then sealed and heated to 180 °C for 24 hours. The resulting product was filtered, washed with deionized water and isopropanol, and then dried at 80 °C for 24 hours. The cathodes were composed of VOH or ZVO active material, super P, and polyvinylidene fluoride (PVDF) in a mass ratio of 7:2:1. N-methyl-2-pyrrolidone (NMP) was used as the dispersant. The slurry mixture was applied to Ti foil, dried at 60 °C for 10 hours under vacuum, and had a mass loading of active materials of 1–2 mg cm^{-2}.

2. Electrochemical Measurements

CR2032 coin-type cells were assembled under ambient conditions. The Zn||Cu half cells utilized glass fiber separators (Whatman GF/A), whereas the Zn||Zn symmetric

cells as well as Zn||VOH and Zn||ZVO full cells employed Whatman GF/D separators. Zn foil (100 μm) was employed as the anode. The electrochemical performance of zinc ion batteries was studied using the LAND Electrochemical Testing System and Solartron Analytical Electrochemical Workstation. Diffusion curves were obtained through chronoamperometry (CA) under a bias voltage of –200 mV over 1000 seconds. Linear sweep voltammetry (LSV) was conducted at a scan rate of 5 mV s^{-1}. Cyclic voltammetry (CV) was conducted at a scan rate of 1 mV s^{-1}. The volume of electrolyte used was controlled at 85 μL.

3. **Material Characterizations**

Scanning Electron Microscopy (SEM): The morphology of the cathode and zinc was examined using a Hitachi SU-8010 SEM at an acceleration voltage of 5 kV. Inductively Coupled Plasma Optical Emission Spectroscopy (ICP-OES): Analytical results were obtained using an Agilent 730 ICP-OES instrument. High Resolution Transmission Electron Microscope (HRTEM) and Energy Dispersive Spectrometer (EDS): HRTEM and EDS measurements were conducted on a JEM-2100F. X-ray Diffraction (XRD): XRD patterns were recorded using a Bruker D8 Advance instrument with Cu Kα radiation (λ=1.5406 Å). Raman Spectroscopy: Raman spectra were acquired using a Horiba Jobin Yvon LabRAM HR Evolution instrument. X-ray Photoelectron Spectroscopy (XPS): XPS analysis was carried out on a Thermo Scientific K-Alpha instrument. All binding energies were referenced to the C 1s peak (284.8 eV). Proton Nuclear Magnetic Resonance (^{1}H-NMR): ^{1}H-NMR spectra were recorded on a BRUKER ASCEND 600 (600 MHz) at room temperature. Contact Angle Measurements: Contact angles were measured using a dataphysics OCA50AF instrument.

4. **Molecular Dynamics (MD) Simulations**

Atomistic MD simulations were performed using the GROMACS[1] (version 2020.6) simulation package. The simulations employed the General Amber force field (GAFF2)

and the TIP3P water model. The Universal Force Field was used for describing the parameters of the ~5.8×5.8 nm^2 $V_2O_5 \cdot H_2O$ surface. Two systems were simulated: one containing 400 $CF_3SO_3^-$, 200 Zn^{2+}, and 5556 water molecules, and the other containing 400 $CF_3SO_3^-$, 200 Zn^{2+}, 134 IDE, and 4440 water molecules. In both cases, the molecules were initially placed in cubic boxes of approximately 6 nm on the $V_2O_5 \cdot H_2O$ (001) surface and then solvated with the specified number of water molecules. The systems underwent energy minimization and equilibration under the NPT ensemble, followed by production runs of 20 ns under the canonical ensemble. Temperature coupling to 298 K was achieved using the Nose-Hoover method, and pressure was coupled to 1 atm using the Parrinello-Rahman method. A cutoff scheme of 1.2 nm was applied for non-bonded interactions, and the Particle Mesh Ewald method[2] with a Fourier spacing of 0.1 nm was used for long-range electrostatic interactions. The LINCS algorithm[3] was used to constrain all covalent bonds involving hydrogen atoms. The distribution of interfacial water was obtained by statistically analyzing the average density distribution over a 20 ns period and subsequently normalizing the results. The two-dimensional imaging is obtained by statistically analyzing the density distribution of water molecules over a 20 ns period.

5. **Density Functional Theory (DFT) Calculation**

DFT calculations were performed using the Vienna Ab initio simulation package (VASP)[4]. The generalized gradient approximation (GGA) with the Perdew, Burke, and Ernzerhof (PBE)[5] exchange-correlation energy was employed. A cutoff energy of 450 eV was used for the plane-wave basis set along with the projector augmented wave (PAW) method[6]. Geometry optimizations were performed with energy and force convergence criteria of 1×10^{-5} eV and 2×10^{-2} eV, respectively. Brillouin zone sampling was conducted using the Monkhorst-Pack scheme, and K-points were generated with VASPkit[7]. The van der Waals interaction was included using the DFT-D3 method[8]. Adsorption energy calculations were based on the equation: $E_{ad} = E_{total} - E_{slab} - E(M)$, where E_{total} is the total energy of the adsorbed state of H_2O or IDE, E_{slab} is the energy of the $V_2O_5 \cdot H_2O$ (001) surface or the energy of Zn(002), and $E(M)$ is the energy of H_2O

or IDE.

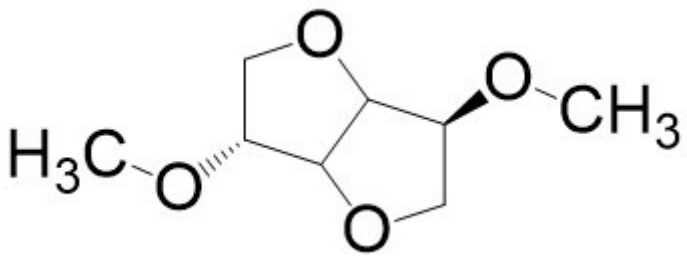

Fig. S1. Chemical structure of IDE.

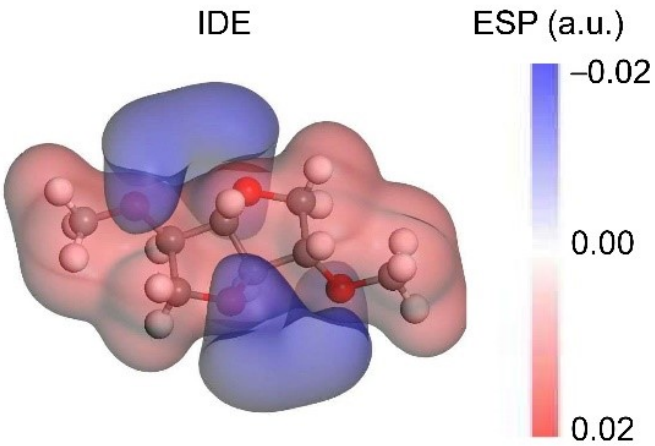

Fig. S2. Electrostatic potential mapping of IDE.

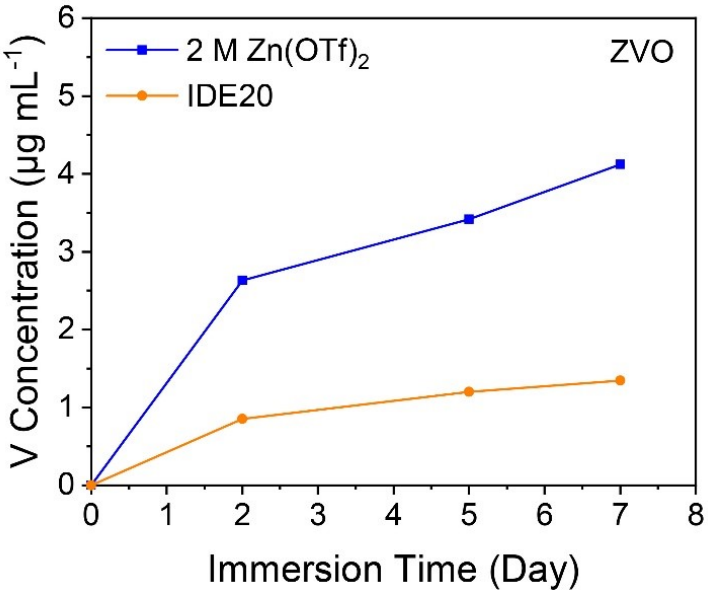

Fig. S3. ICP-OES results of electrolytes with ZVO cathodes immersing at various time.

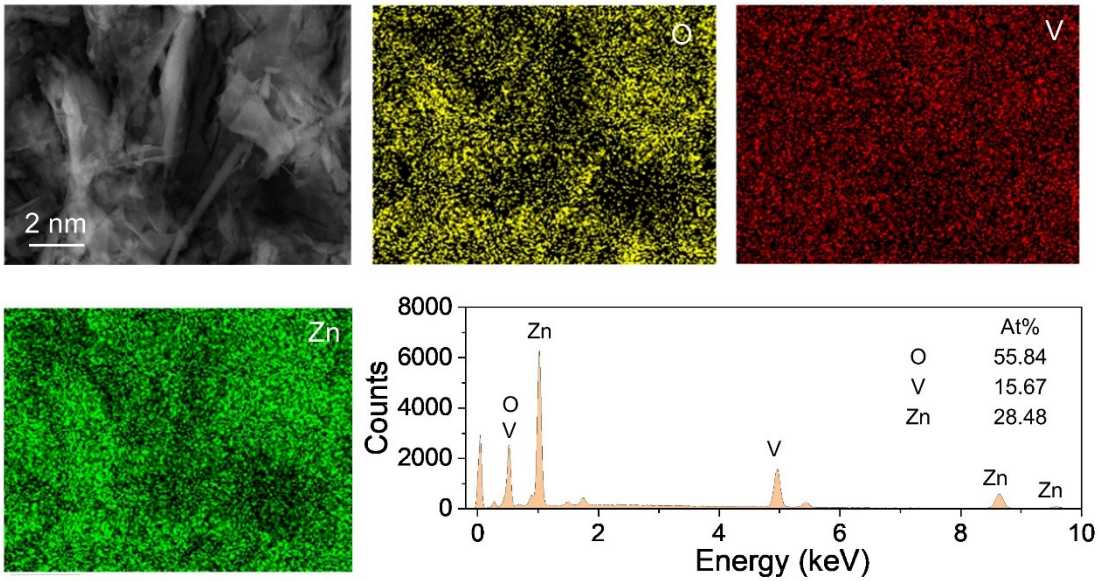

Fig. S4. EDS mapping of corresponding SEM images of VOH cathodes after cycling with 2 M $Zn(OTf)_2$ for 5 cycles at 5 A g^{-1}.

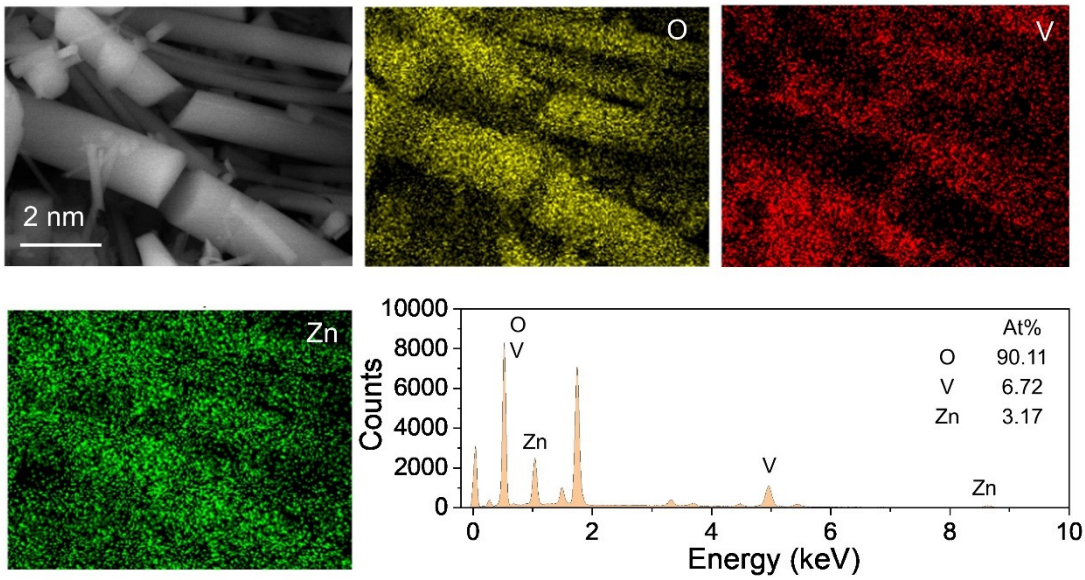

Fig. S5. EDS mapping of corresponding SEM images of VOH cathodes after cycling with IDE20 for 5 cycles at 5 A g^{-1}.

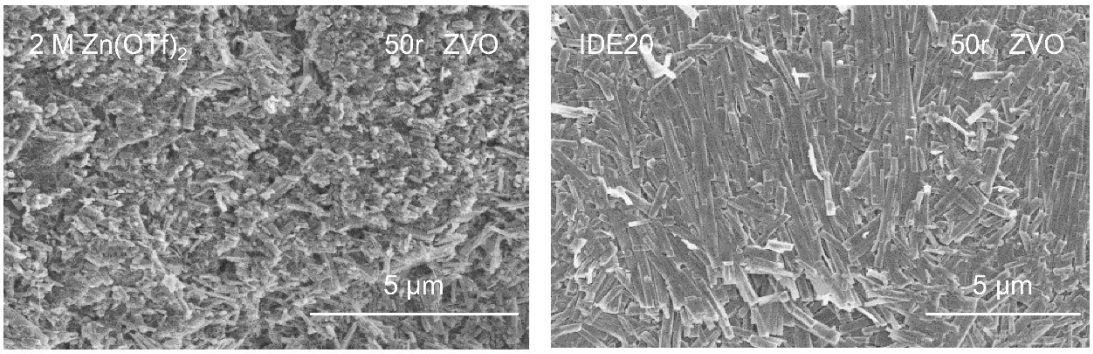

Fig. S6. SEM images of ZVO cathodes using 2 M $Zn(OTf)_2$ and IDE20 electrolytes after 50 cycles.

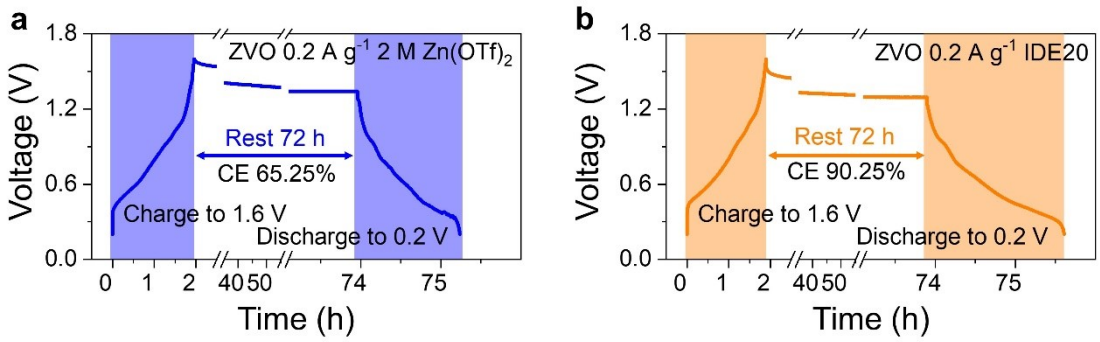

Fig. S7. Self-discharge analysis of ZVO cathodes using 2 M $Zn(OTf)_2$ and IDE20 electrolytes.

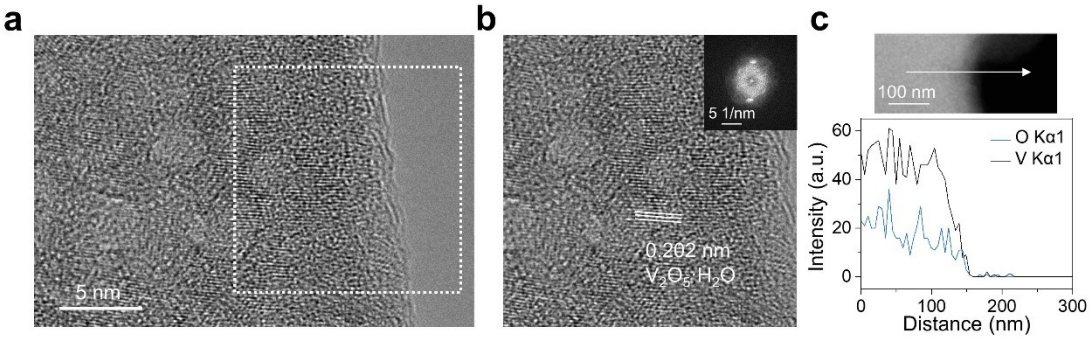

Fig. S8. (a) HRTEM image of VOH powder. (b) HRTEM image of selected region in a and corresponding FFT pattern. (c) EDS line scanning of the corresponding images of VOH cathodes.

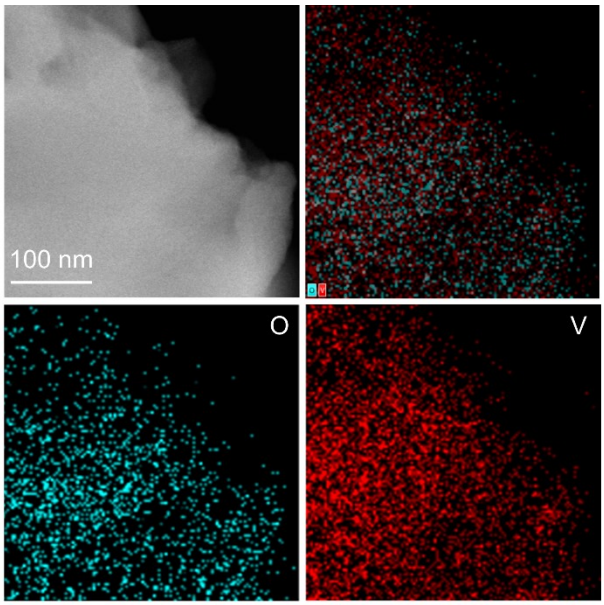

Fig. S9. EDS mapping of corresponding TEM images of VOH powder from surface to subsurface regions.

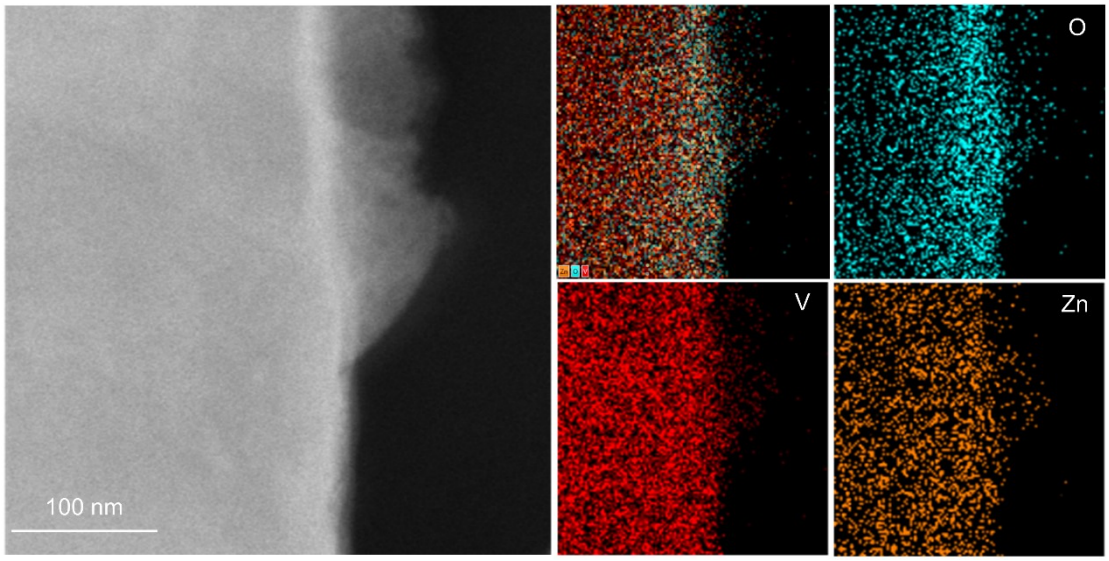

Fig. S10. EDS mapping of corresponding TEM images of VOH cathodes after cycling with 2 M $Zn(OTf)_2$ for 20 cycles at 5 A g^{-1} from surface to subsurface regions.

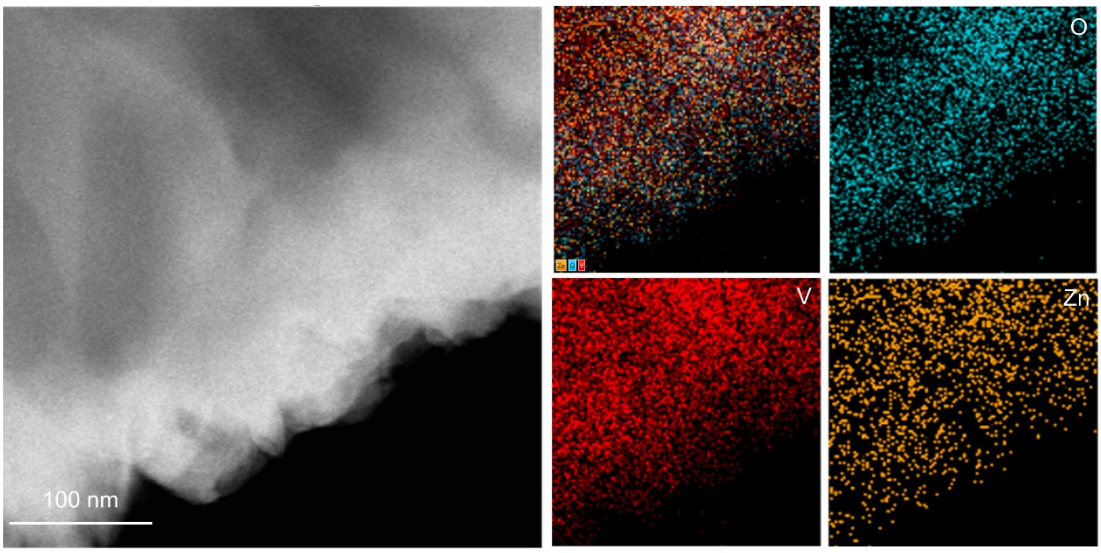

Fig. S11. EDS mapping of corresponding TEM images of VOH cathodes after cycling with IDE20 for 20 cycles at 5 A g^{-1} from surface to subsurface regions.

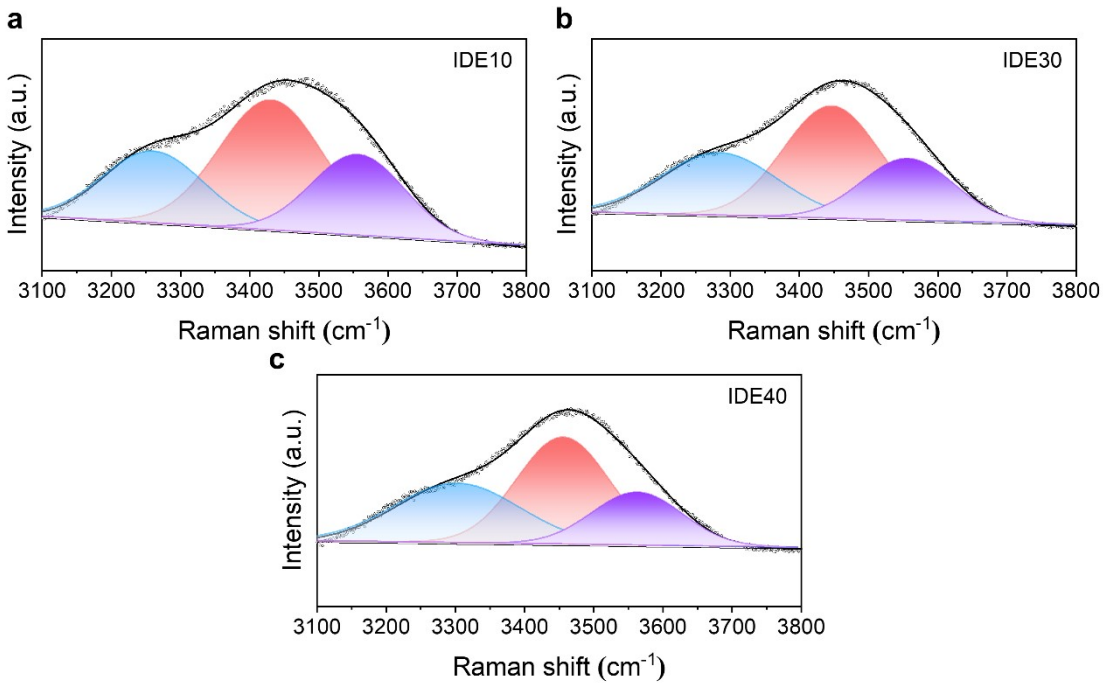

Fig. S12. Fitted Raman spectra of (a) IDE10, (b) IDE30 and (c) IDE40 in the region of O-H stretching.

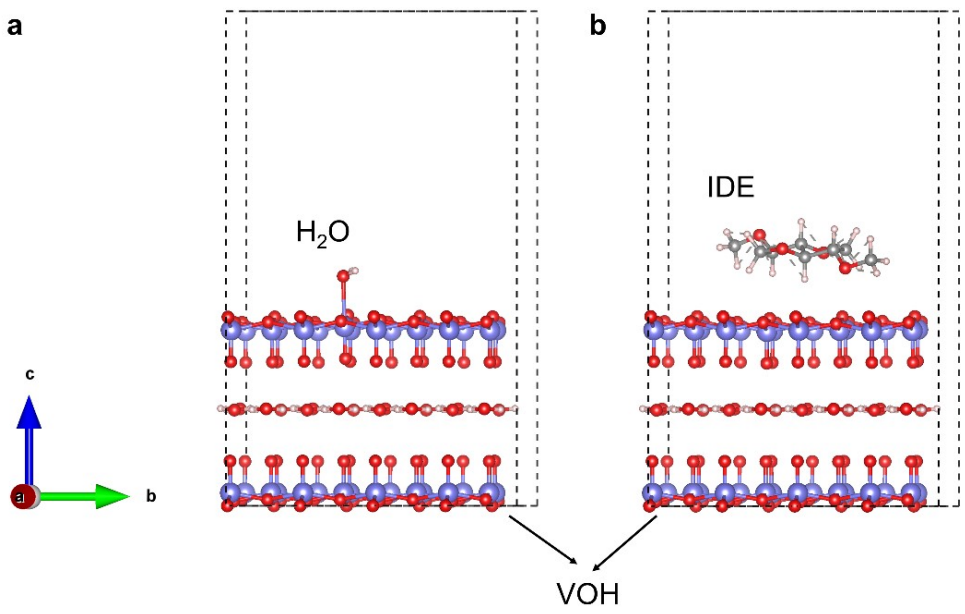

Fig. S13. Adsorption of H_2O and IDE on VOH cathode.

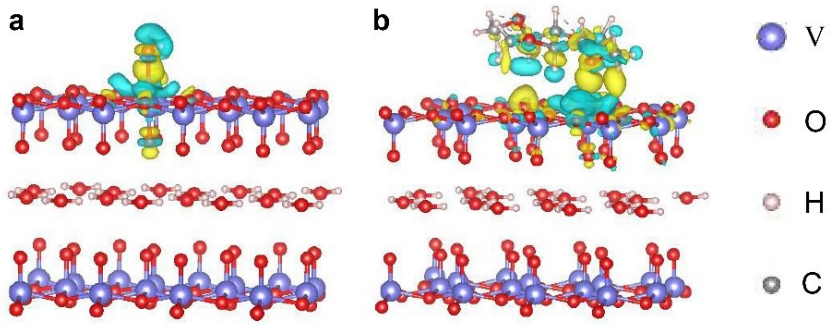

Fig. S14. Differential charge density diagram of H_2O and IDE at VOH cathode interface. (Yellow indicates a rise in charge density, while blue indicates a fall in charge density.)

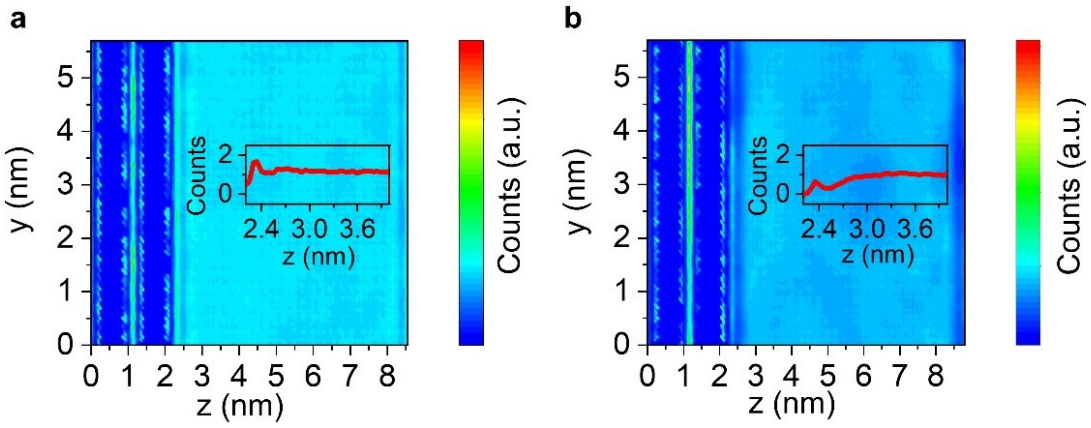

Fig. S15. Cross-section of the water density distribution from the surface of VOH cathode to bulk electrolytes in (a) 2 M $Zn(OTf)_2$ and (b) IDE20 electrolytes, respectively. The inset shows the distribution of water along the z-axis at y = 3 nm.

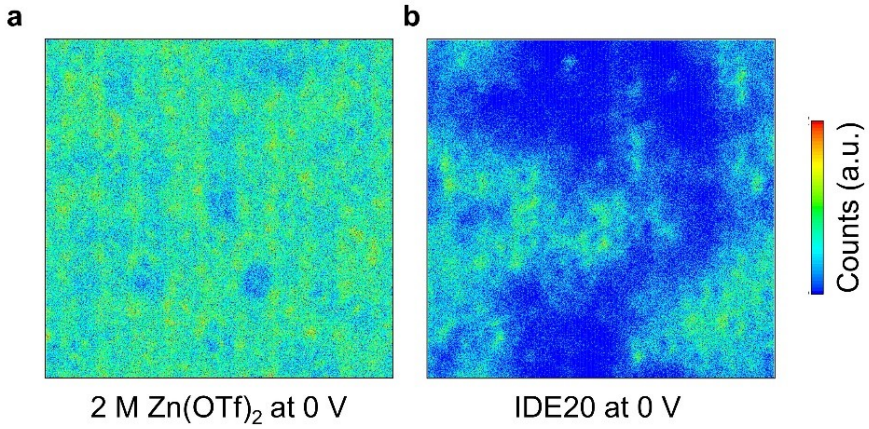

Fig. S16. 2D density distribution of interfacial H_2O at VOH cathode.

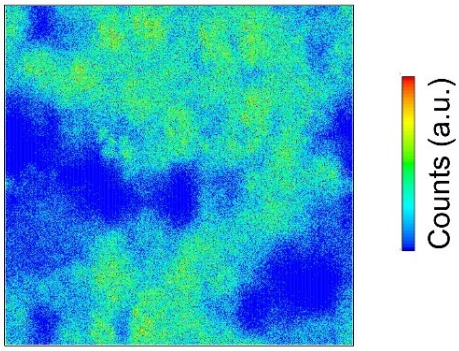

IDE20 at 0 V

Fig. S17. 2D density distribution of interfacial IDE at VOH cathode.

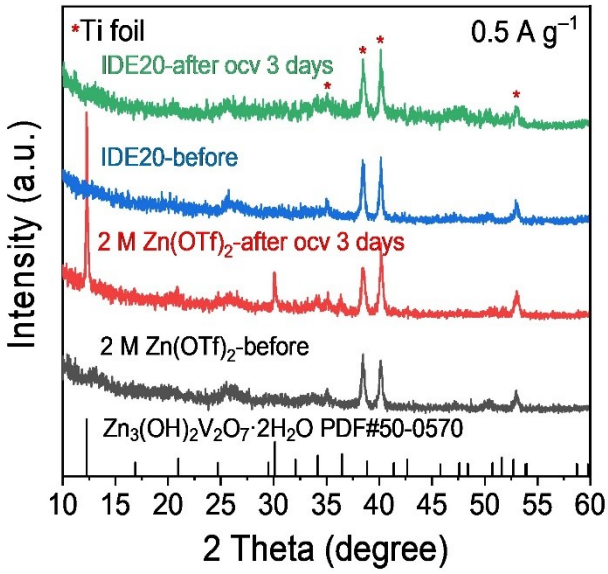

Fig. S18. XRD patterns of VOH cathodes cycled under 2 M $Zn(OTf)_2$ and IDE20 electrolytes before and after OCV 3 days.

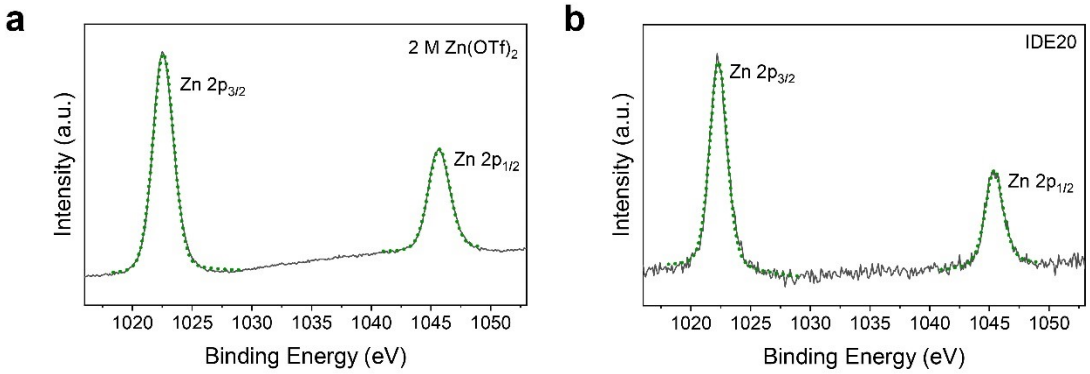

Fig. S19. XPS fitted curves of the Zn element of the VOH cathodes after cycling in (a) 2 M $Zn(OTf)_2$ and (b) IDE20 electrolytes.

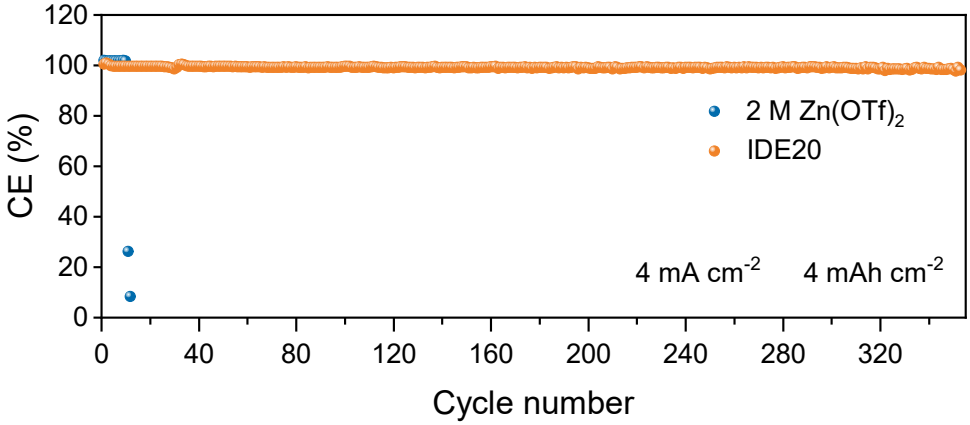

Fig. S20. CE measurements of asymmetric Zn||Cu cells with different electrolytes at 4 mA cm^{-2}, 4 mAh cm^{-2}.

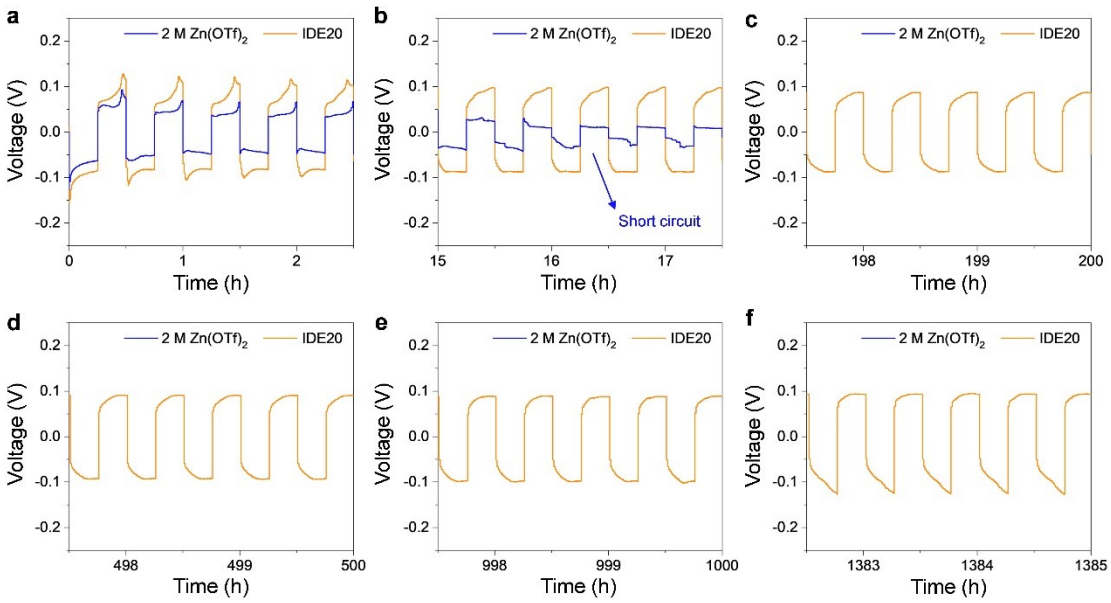

Fig. S21. The amplified profile of Fig. 5b at different cycles.

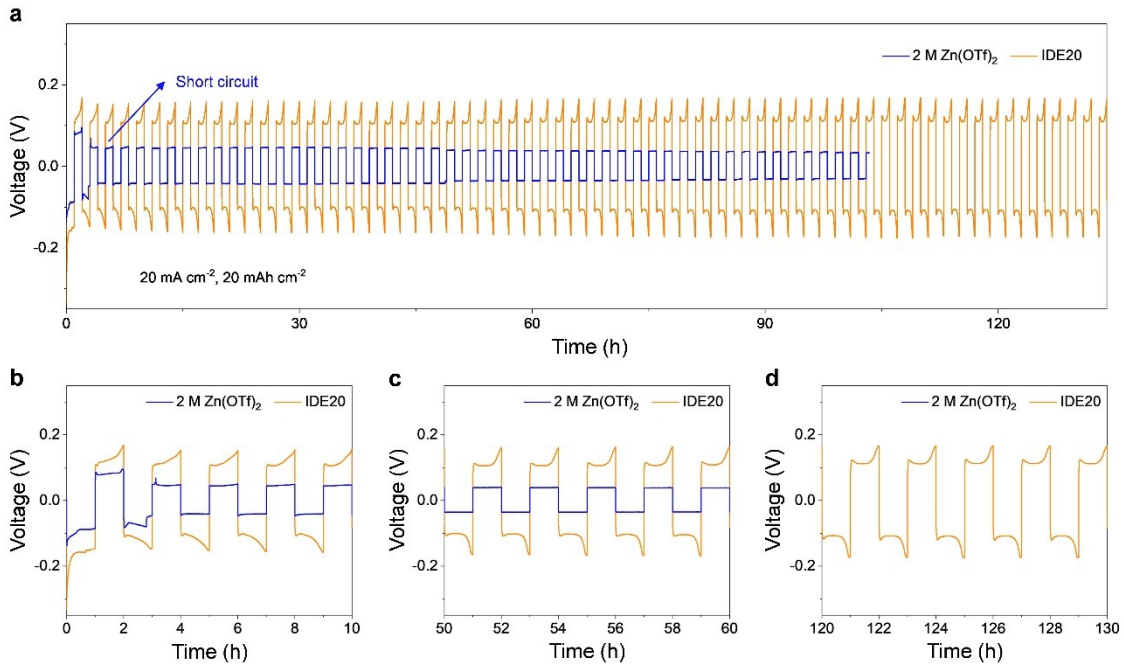

Fig. S22. (a) Galvanostatic cycling stability of symmetric Zn||Zn cells under 20 mA cm^{-2}, 20 mAh cm^{-2}. Enlarged view of (b) 1-5 cycles, (c) 25-30 cycles, (d) 60-65 cycles.

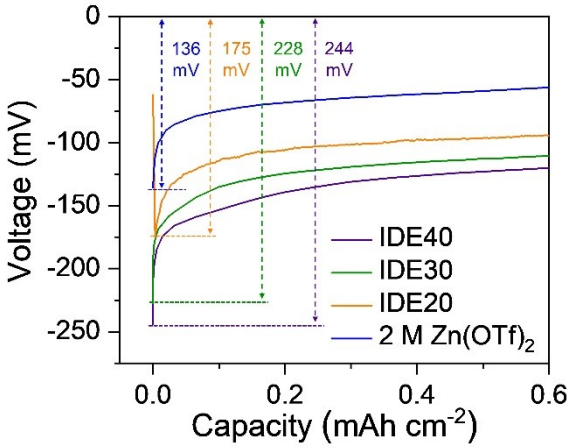

Fig. S23. Nucleation overpotentials for cells using 2 M $Zn(OTf)_2$, IDE20, IDE30 and IDE40 electrolytes.

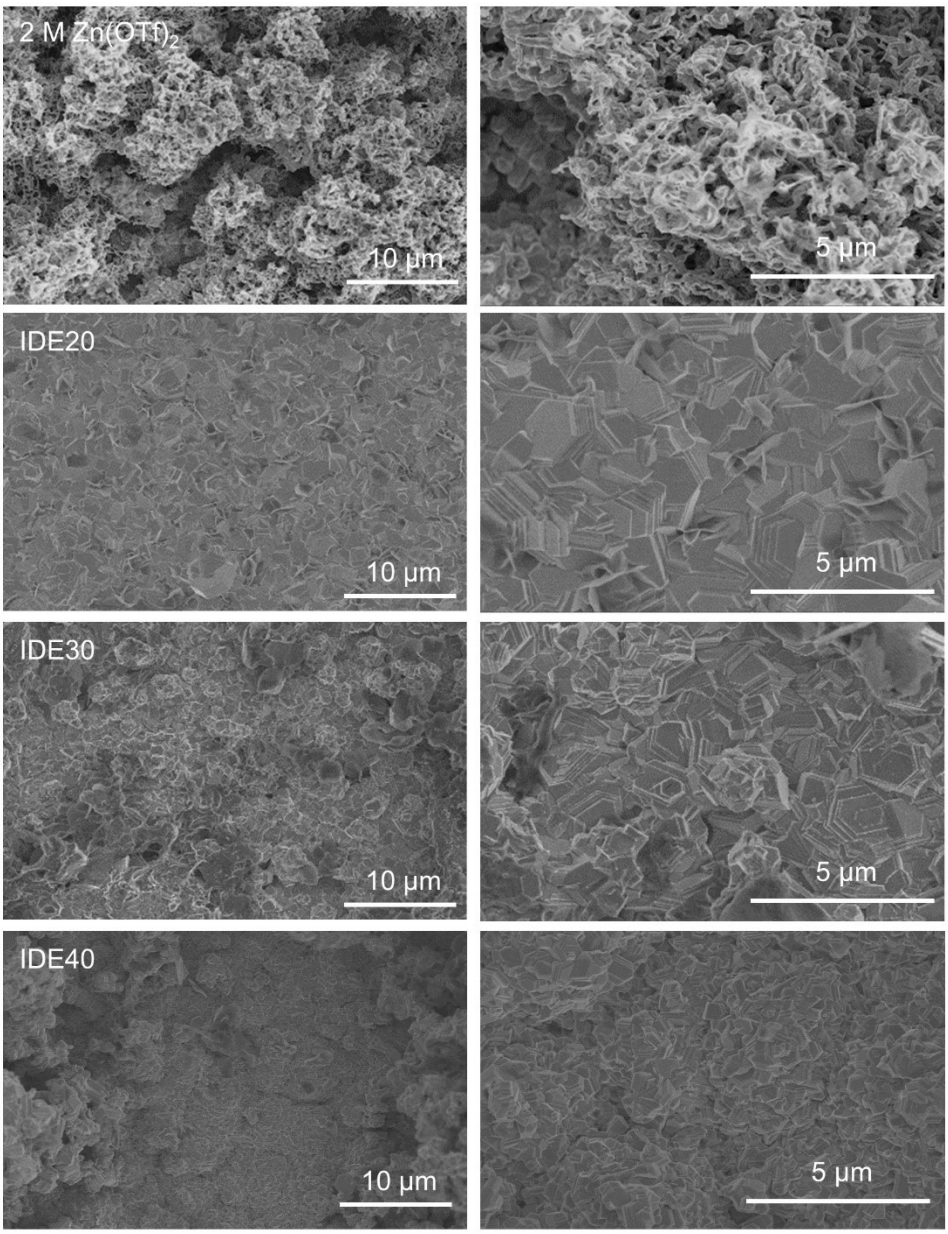

Fig. S24. Surface morphology of deposited zinc in 2 M $Zn(OTf)_2$, IDE20, IDE30 and IDE40 electrolytes.

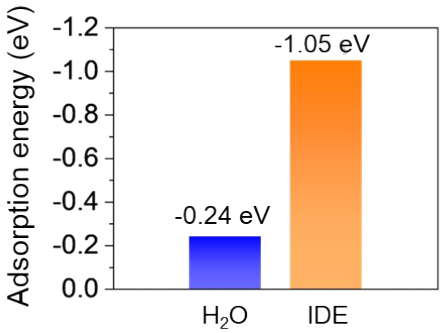

Fig. S25. Adsorption Energy of H_2O and IDE on Zn anode.

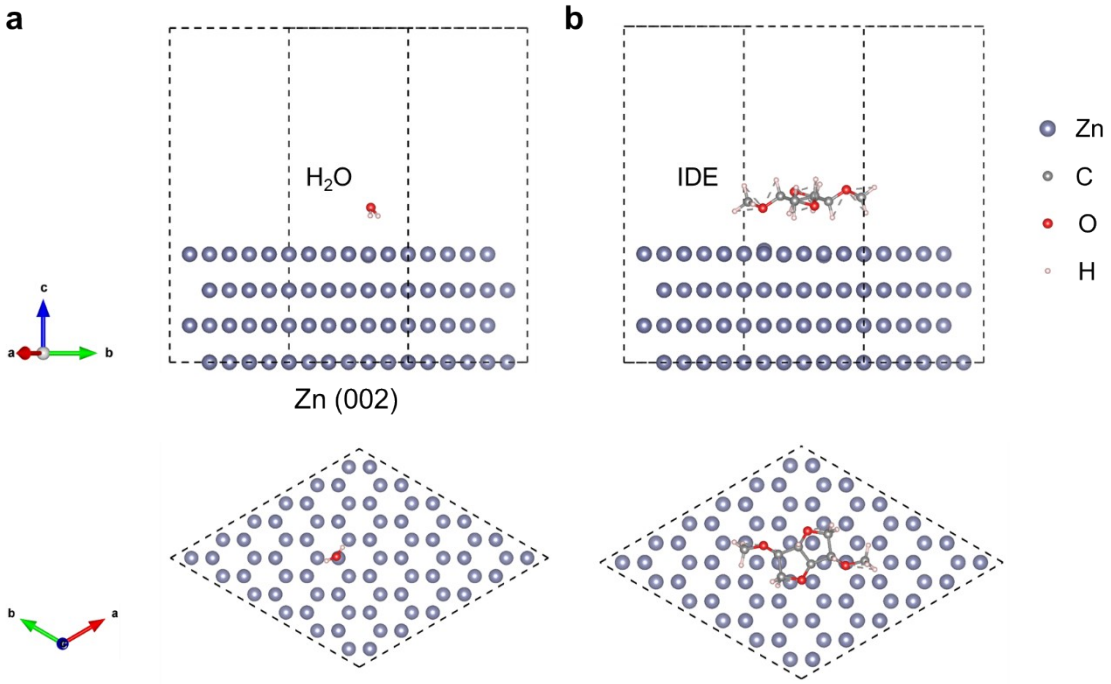

Fig. S26. Adsorption of H_2O and IDE on Zn anode.

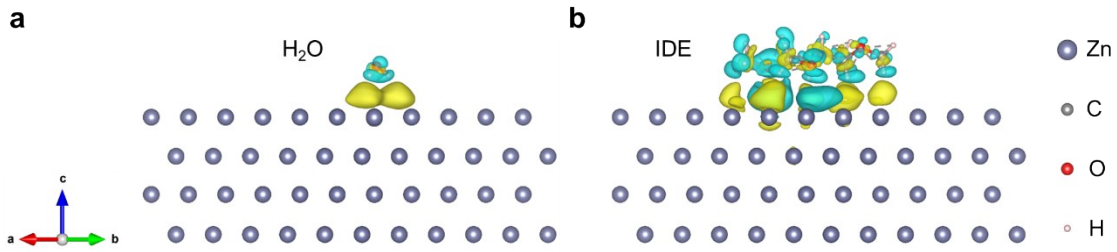

Fig. S27. Differential charge density diagram of H_2O and IDE at Zn anode interface. (Yellow indicates a rise in charge density, while blue indicates a fall in charge density.)

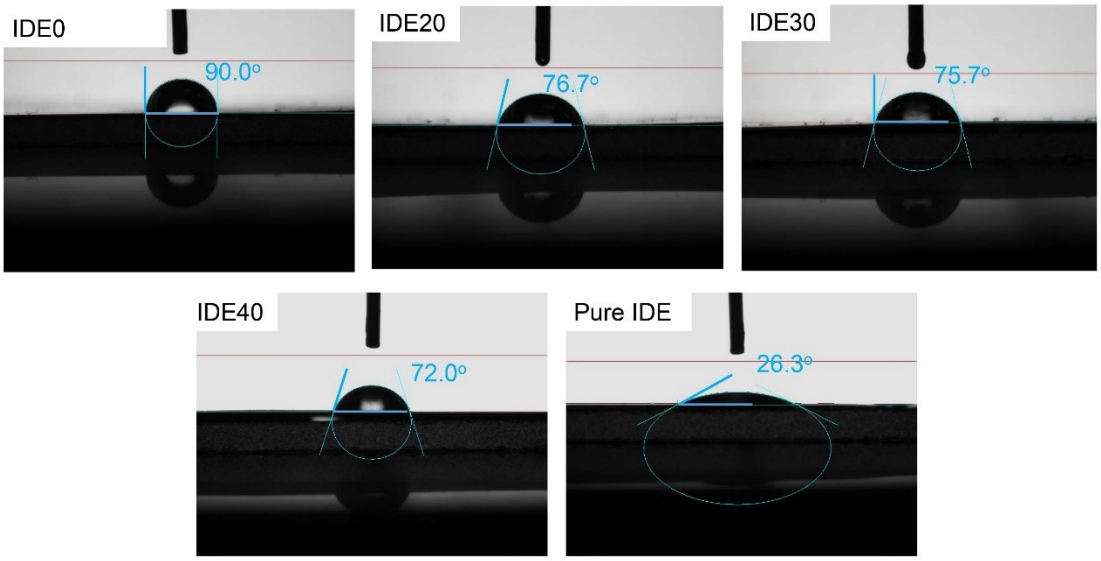

Fig. S28. Contact angle of IDE0, IDE20, IDE30 , IDE40 and pure IDE on zinc foil.

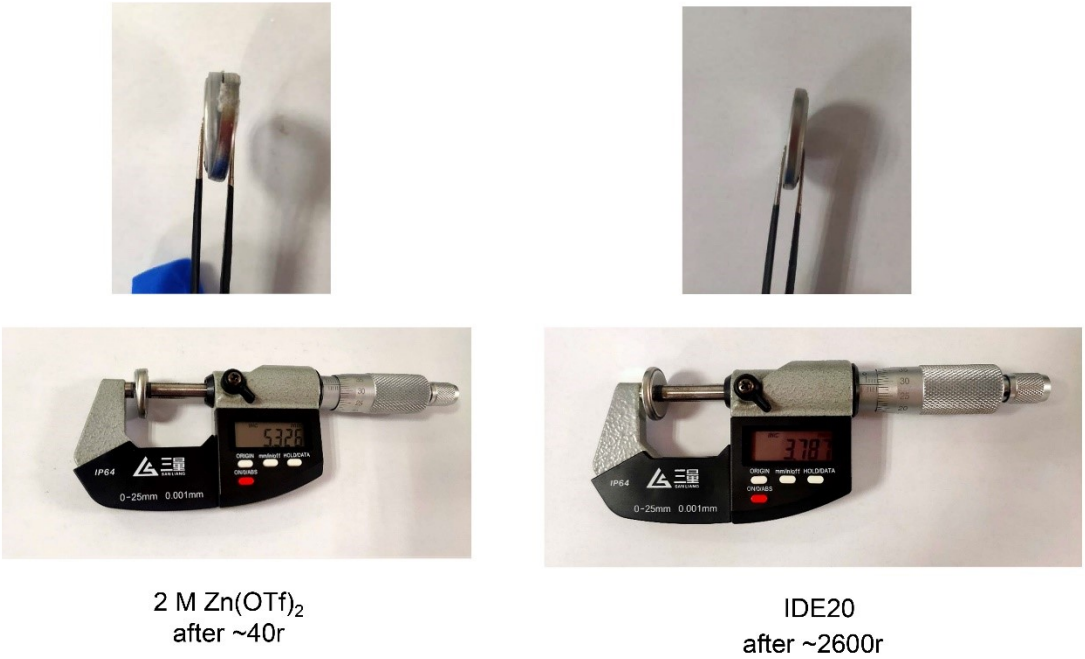

2 M $Zn(OTf)_2$
after ~40r

IDE20
after ~2600r

Fig. S29. Optical photograph of the battery case thickness measurement at the end of the cycle.

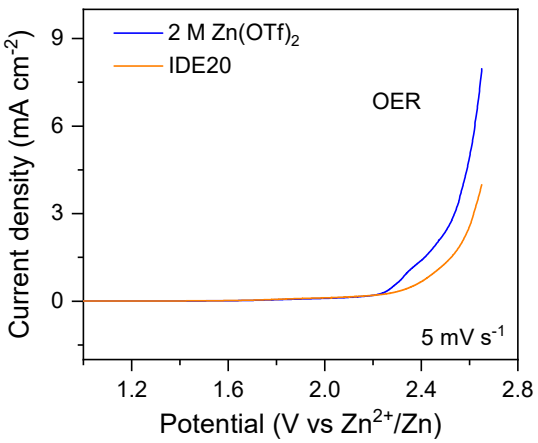

Fig. S30. LSV characterization in 2 M $Zn(OTf)_2$ and IDE20 electrolytes.

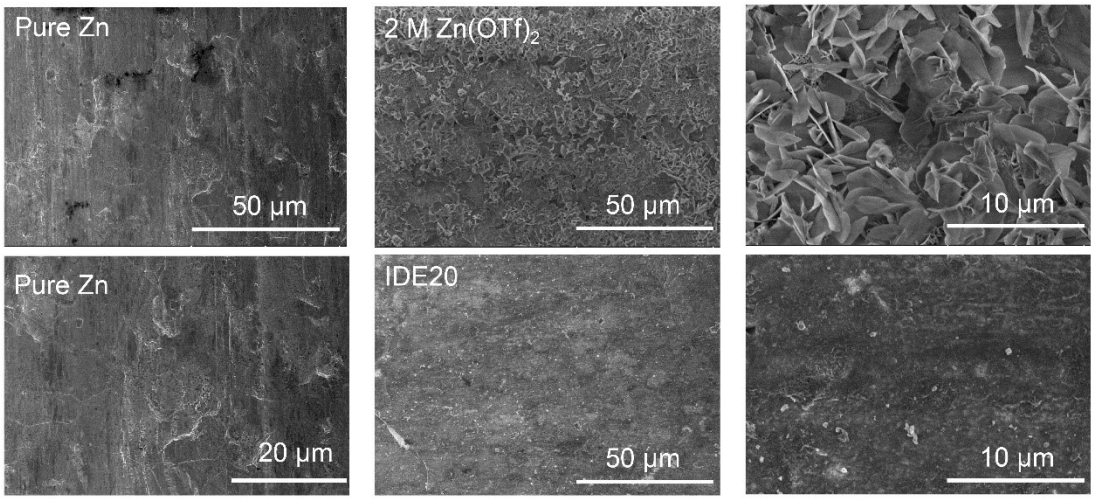

Fig. S31. SEM images of zinc foil after soaking for 3 days.

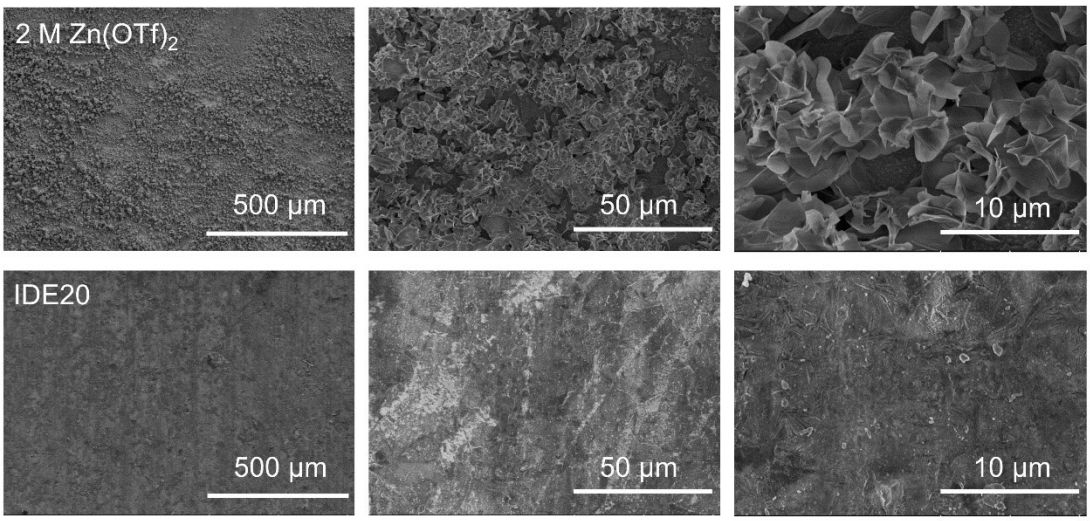

Fig. S32. SEM images of Zn foil after soaking for 5 days.

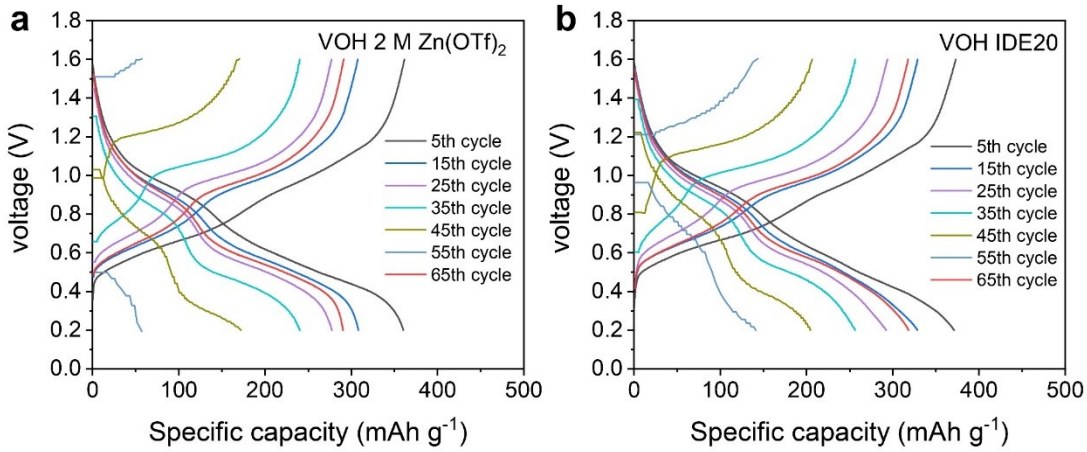

Fig. S33. Charge/discharge curve for Zn||VOH battery using (a) 2 M $Zn(OTf)_2$ and (b) IDE20 electrolytes at different rates.

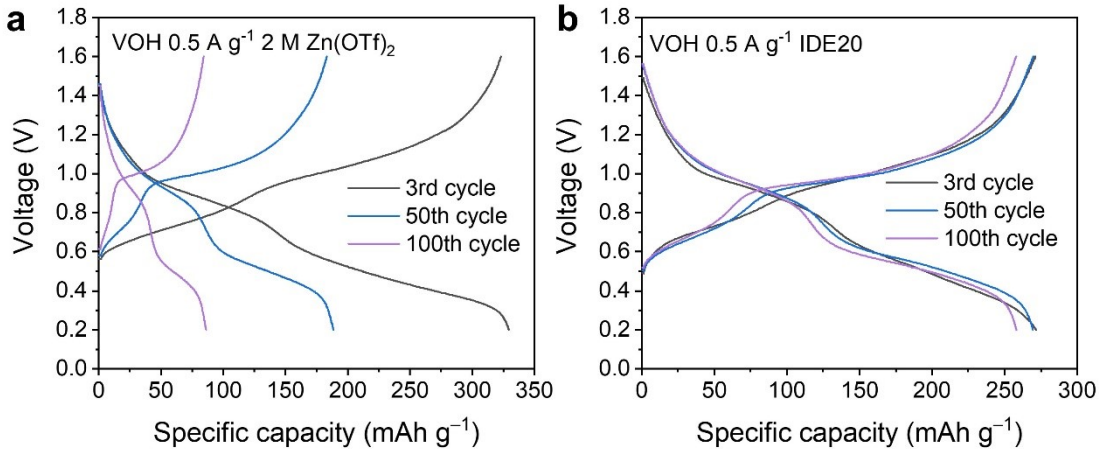

Fig. S34. Charge/discharge curve for Zn||VOH battery using (a) 2 M $Zn(OTf)_2$ and (b) IDE20 electrolytes.

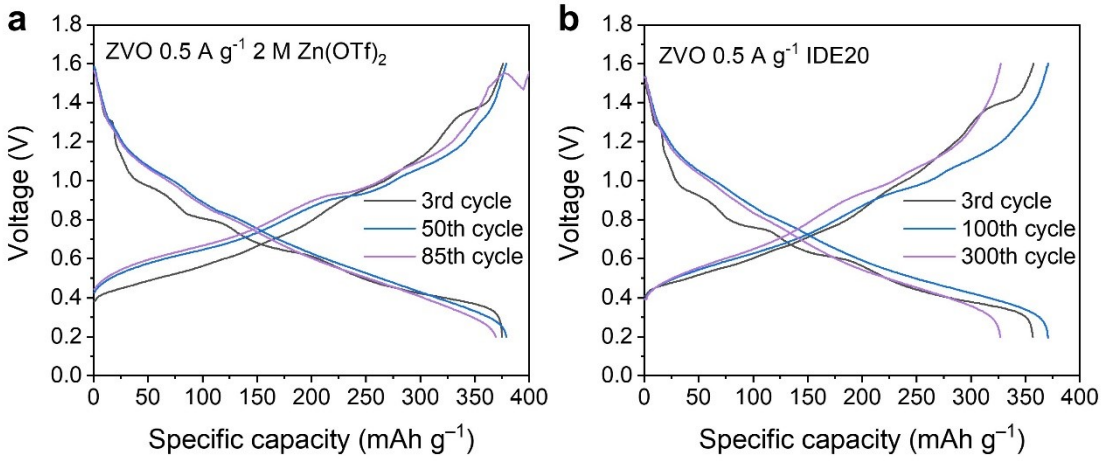

Fig. S35. Charge/discharge curve for Zn||ZVO battery using (a) 2 M $Zn(OTf)_2$ and (b) IDE20 electrolytes.

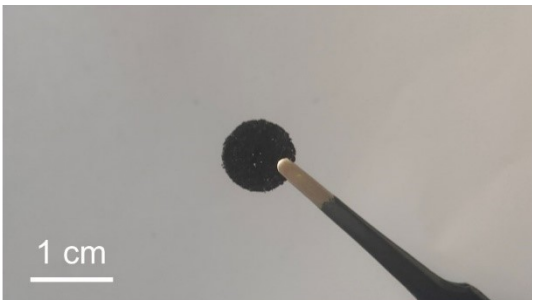

Fig. S36. Optical photograph of high mass loading VOH cathodes.

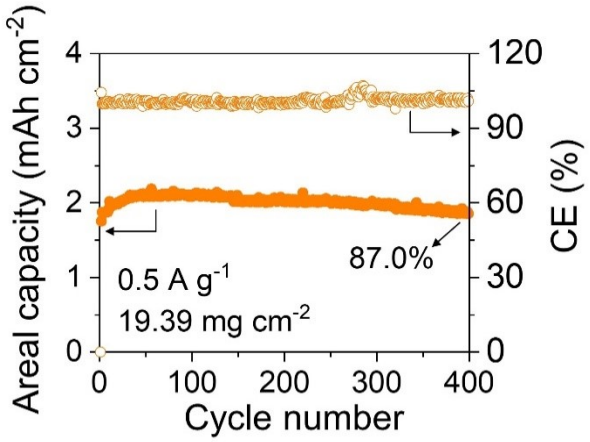

Fig. S37. Cycling stability of Zn||VOH full cells using high mass loading VOH cathodes (19.39 mg cm^{-2}).

Table S1. R_{ct} values of VOH||VOH cells with 2 M $Zn(OTf)_2$ and IDE20 electrolytes, respectively, at different temperatures.

Temperature (°C)	R_{ct} (ohm, using 2 M $Zn(OTf)_2$)	R_{ct} (ohm, using IDE20)
30	74.0	46.0
40	36.0	33.5
50	32.0	28.0
60	24.0	27.0
70	16.6	21.1

Table S2. Electrochemical performances of aqueous zinc-ion batteries assembled with V-based cathodes reported recently.

Cathode material	Current density (A g^{-1})	Capacity (mAh g^{-1})	Electrolyte formulation	Ref.
$V_2O_5 \cdot nH_2O$	5	210.1	**IDE20**	**This work**
	2	257.8		
	1	294.0		
	0.5	331.6		
	0.2	377.8		
$Zn_{0.25}V_2O_5 \cdot nH_2O$	5	270.2		
	2	360.1		
	1	381.2		
	0.5	389.2		
	0.2	392.8		
VS_2@SS	1	97.0	2 M $ZnSO_4$+5% NMP	Ref. 23
$V_2O_5 \cdot 1.6H_2O$/MXene	0.5	~150	$Zn(OTf)_2$+80%TEP	Ref. 35
$NH_4V_4O_{10}$	2	111.5	$ZnSO_4$+ (aminomethyl)phosphonic acid	Ref. 44
$Zn_{0.25}V_2O_5 \cdot nH_2O$	1.5	~160	3 M $Zn(OTf)_2$+63 wt% sulfolane	Ref. 45
V_2O_5	1	~180	2 M $ZnSO_4$+g-C_3N_4 QDs	Ref. 46
$NaV_3O_8 \cdot 1.5H_2O$	0.3	~250	1 M $Zn(OTf)_2$ dissolved in DMAC/TMP/H_2O (5:2:3) mixture	Ref. 47
V_2O_5	5	127.9	3 M $ZnSO_4$+5 mM hexamethyle netetramine	Ref. 48

References

1. B. Hess, C. Kutzner, D. van der Spoel and E. Lindahl, *J. Chem. Theory Comp.*, 2008, **4**, 435–447.
2. U. Essmann, L. Perera, M. L. Berkowitz, T. Darden, H. Lee and L. G. Pedersen, *J. Chem. Phys.*, 1995, **103**, 8577-8593.
3. B. Hess, H. Bekker, H. J. C. Berendsen and J. G. E. M. Fraaije, *J. Comput. Chem.*, 1997, **18**, 1463-1472.
4. G. Kresse and J. Furthmüller, *Phys. Rev. B*, 1996, **54**, 11169-1118.
5. J. P. Perdew, K. Burke and M. Ernzerhof, *Phys. Rev. Lett.*, 1996, **77**, 3865-3868.
6. G. Kresse and D. Joubert, *Phys. Rev. B*, 1999, **59**, 1758-1775.
7. V. Wang, N. Xu, J.-C. Liu, G. Tang and W.-T. Geng, *Comput. Phys. Commun.*, 2021, **267**, 108033.
8. S. Grimme, J. Antony, S. Ehrlich and H. Krieg, *J. Chem. Phys.*, 2010, **132**, 154104.